Thin Solid Films 558 (2014) 200–207

Contents lists available at ScienceDirect

Thin Solid Films

journal homepage: www.elsevier.com/locate/tsf

Preparation and characterization of polymeric thin films containing gold nanoshells via electrostatic layer-by-layer self-assembly

Sang Ho Lee, Andrew C. Jamison, David M. Hoffman *, Allan J. Jacobson **, T. Randall Lee ***

Department of Chemistry and Texas Center for Superconductivity, University of Houston, 4800 Calhoun Road, Houston, TX 77204-5003, United States

ARTICLE INFO

Article history:
Received 27 May 2013
Received in revised form 1 February 2014
Accepted 5 February 2014
Available online 15 February 2014

Keywords:
Gold nanoshells
Layer-by-layer self-assembly
Polyethyleneimine films
Solar energy
Nanoshell aggregation

ABSTRACT

As an initial step in the development of surfaces for collecting thermal energy, gold shell/silica core particles (~200 nm in diameter with shells ~25 nm thick) were synthesized and incorporated into organic polymeric thin films. The morphologies of these nanoshells were characterized with scanning and transmission electron microscopy. Powder X-ray diffraction demonstrated that the gold layers were highly crystalline. Thin films containing the gold nanoshells and polyethyleneimine were generated using dip-coating techniques based on electrostatic layer-by-layer self-assembly methods. Scanning electron microscopy was used to image the resultant composite films, which contained uniformly distributed gold nanoshells with limited aggregation. The optical properties were analyzed by absorption spectroscopy, revealing broad extinctions ranging from the visible to the near-IR spectral regions. X-ray photoelectron spectroscopy spectra were also obtained to determine the elements present and the oxidation states of these elements.

1. Introduction

Metal nanoparticles (NPs) derived from noble metals have drawn wide interest because of their unique and tunable optical properties and their efficient photo-thermal effects [1]. The most notable optical feature of these NPs is their surface plasmon resonance (SPR), which arises from an interaction between an electromagnetic wave and the conduction electrons present in the metal. Under the irradiation of light, electrons near the surface of the metal NPs are driven by the light wave's electric field to oscillate collectively when the frequency of the optical excitation matches their natural frequency, a process that also leads to a maximum of energy absorption [2,3]. The peak position of the SPR band for metal nanoparticles varies with the particle size, shape, and composition, along with the refractive index of the surrounding medium [4–8]. Studies of this enhanced absorption of light have included investigations of heat generation by metal NPs under illumination, an associated physical property [9,10]. Because the absorption of incident photons is greatest when the light produces a resonance response, the conversion of photon energy into heat energy, as well as the heat transfer from the NPs to the surrounding matrix, can be maximized for a metal NP system through prudent NP design. The heating effect is especially strong for metal NPs because they have a high optical quantum yield (i.e., they are poor emitters of light). Analyses of this heating effect have included efforts to measure the temperature on the surface of gold nanoparticles (AuNPs) when they are optically excited [9,10].

One effort to modify the wavelength at which an NP system absorbs light has been through the development of shell/core metal nanoparticles called "nanoshells" [5,7,11,12]. Gold nanoshells (AuNSs) consist of a spherical dielectric core, such as silica or polystyrene, surrounded by a thin gold shell. Most metal NPs that exhibit SPR behavior generally adsorb or scatter light over the ultraviolet and visible regions of the electromagnetic spectrum. In contrast, the SPR of AuNSs can be tuned to a wider range of frequencies than typical AuNPs, ranging from the ultraviolet to the near-infrared regions of the electromagnetic spectrum. AuNSs having SPRs in the near infrared region are well suited for hyperthermia applications in biological systems because biological fluids and tissue are transparent over this range of the electromagnetic spectrum. Apart from their optical properties, AuNSs are biologically inert and their surfaces can be readily functionalized with selective biomolecular linkers for the purpose of targeting them to specific sites of interest [13]. Some potential applications that have been explored that rely on their optical and thermal properties include biological imaging and detection, drug delivery, and the photothermal treatment of various diseases, such as cancer [14–18]. The most common synthetic approach for producing AuNSs has been the "seeded-growth" method [5,11]. This route involves the synthesis of silica NPs and the functionalization of their surface with terminal amine groups to facilitate the attachment of much smaller colloidal gold particles, which then serve as seeds to template the subsequent growth of a polycrystalline gold shell in a controlled manner.

* Corresponding author. Tel.: +1 713 743 3255.
** Corresponding author. Tel.: +1 713 743 2785.
*** Corresponding author. Tel.: +1 713 743 2724.
E-mail addresses: hoffman@uh.edu (D.M. Hoffman), ajjacob@uh.edu (A.J. Jacobson), trlee@uh.edu (T.R. Lee).

http://dx.doi.org/10.1016/j.tsf.2014.02.021
0040-6090/

The utilization of nanoshells in device architectures has also been pursued [19,20]. In particular, an assembled layer of nanoparticles to generate thin-film structures has many promising applications, including the incorporation of functional layers in optoelectronic devices, the development of efficient electrodes for fuel cells, and the improvement of biosensor performance [21–26]. Zhang et al. have reported the fabrication of multilayered AuNP thin films on aminosilane-functionalized quartz substrates [25]. These researchers showed that the use of layer-by-layer (LBL) assembly with poly(allylamine hydrochloride) afforded tightly packed AuNPs; however, the NPs began to agglomerate and form large clusters with an increase in the number of assembled layers. Separately, Shao-Horn and co-workers reported the fabrication of composite thin films composed of AuNPs and multiwalled carbon nanotubes using electrostatic LBL assembly [22]. These researchers fabricated thin films by the assembly of positively charged 2-aminoethanethiol-stabilized AuNPs together with negatively charged carboxylic acid functionalized-multiwalled carbon nanotubes on an organosilane-modified ITO electrode.

In this manuscript, we describe a process for the fabrication of polymeric thin films containing AuNSs. These composite materials are being developed for use in solar-thermal collectors [27], a project which complements separate efforts that target the use of AuNSs for plasmon-enhanced dye-sensitized solar cells [28]. In the present study, in order to optimize light exposure for these surface-bound metal particles, AuNSs dispersed within polyethyleneimine (PEI) films were prepared via electrostatic layer-by-layer assembly using simple dip-coating techniques. Specifically, a thin film of water-soluble PEI was adsorbed onto a glass microscope slide, and then negatively charged AuNSs were absorbed electrostatically from aqueous solution onto the positively charged surface. The process could be repeatedly cycled to increase the thickness of the film in a controlled manner. The use of PEI was particularly effective for particle dispersion because the polymer readily absorbed on the substrate and allowed only limited aggregation of the nanoshells.

2. Experimental section

2.1. Synthesis of silica nanoparticles and functionalization of the surface

Ammonia (3.0 mL, 30% NH_3 as NH_4OH assay) was added to ethanol (50 mL). The mixture was stirred vigorously, and 1.5 mL of tetraethyl orthosilicate (TEOS) was added dropwise. Over the course of 30 min, the solution changed from clear to opaque white. An excess of (3-aminopropyl)trimethoxysilane (APTMS, ~0.5 mL) was then added to the vigorously stirred silica nanoparticle solution. The mixture was stirred for 2 h, and then gently refluxed for an additional 1 h to enhance covalent bonding of the APTMS groups to the silica nanoparticle surface. The APTMS-coated silica nanoparticles were isolated by centrifuging the mixture and then redispersing in ethanol.

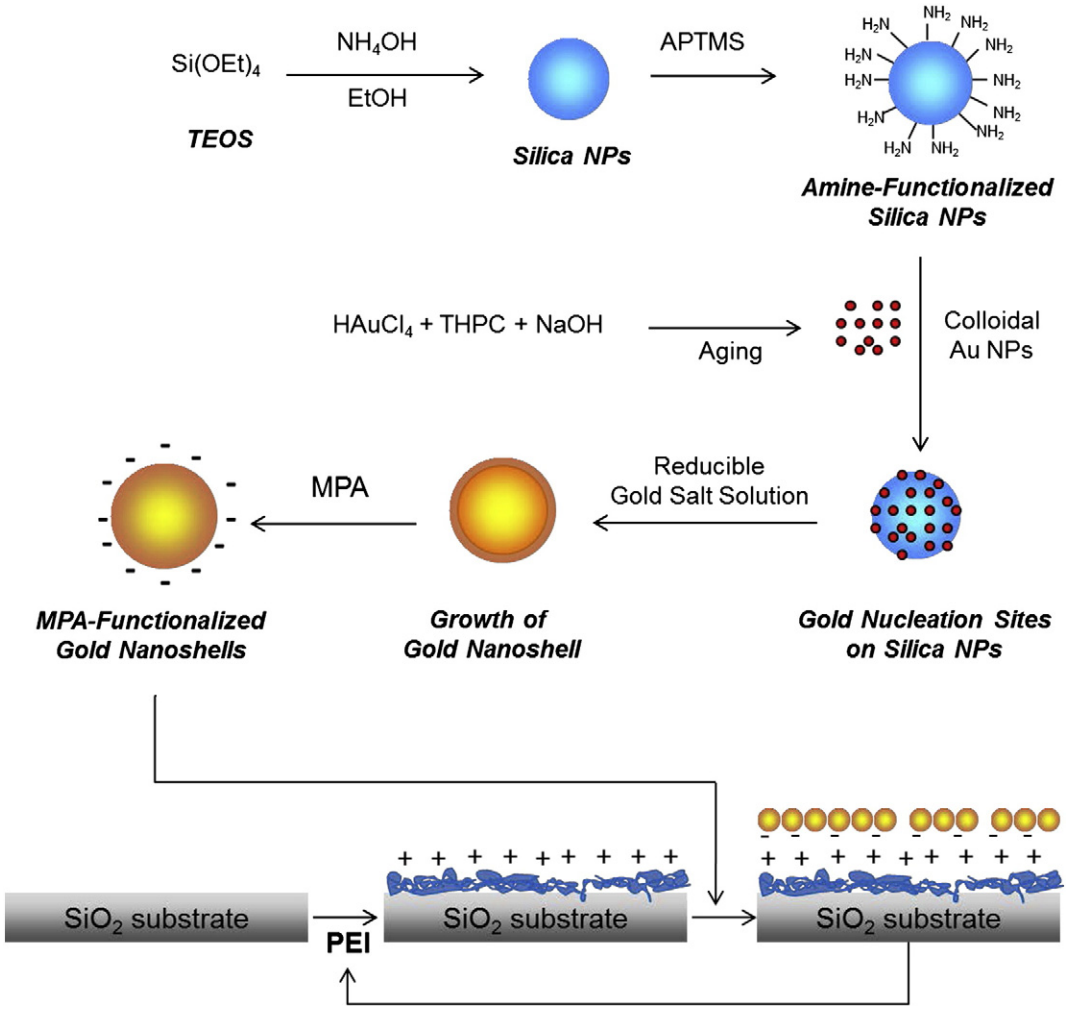

Scheme 1. Preparation of gold nanoshells; acronyms are defined in the Experimental section.

2.2. Preparation of a solution of colloidal gold nanoparticles

Tetrakis(hydroxylmethyl)-phosphonium chloride (THPC) solution was prepared by adding 12 μL of 80% THPC in water to 1 mL of HPLC grade water. An aliquot of 1 M NaOH (0.5 mL) and 1 mL of THPC solution were added to 45 mL of HPLC grade water. The mixture was vigorously stirred for 5 min, and 2 mL of 1% hydrogen tetrachloroaurate(III) ($HAuCl_4$) solution (1 g $HAuCl_4$ in 100 mL of water) was quickly added to the stirred solution to afford the colloidal gold NPs.

2.3. Addition of colloidal gold to the functionalized silica nanoparticles

The colloidal gold NP solution prepared above was concentrated by rotary evaporation to a volume of 13 mL. In a 45-mL centrifuge tube, 1 mL of the APTMS-functionalized silica NP solution was added to an excess (10 mL) of the concentrated AuNP solution. The mixture was vigorously shaken, and then transferred to a refrigerator (~4 °C) and stored overnight. The solution was then centrifuged (3000 rpm, 1 h), and red-colored particles were observed to settle at the bottom of the centrifuge tube. The particles were isolated and redispersed by sonication in HPLC grade water. The solution was then centrifuged again (3000 rpm, 1 h), and the isolated particles were washed twice with HPLC grade water. The purified particles were redispersed in 7.5 mL of HPLC grade water to give a gold-seeded silica nanoparticle stock solution.

2.4. Preparation of a reducible gold salt solution (K-Gold)

In a 500 mL round-bottomed flask, potassium carbonate (0.1 g) was dissolved in 400 mL of HPLC grade water. After stirring for 10 min, 8 mL of 1% $HAuCl_4$ solution (1 g $HAuCl_4$ in 100 mL of water) was added. The solution initially appeared yellow but slowly became colorless over the course of ~12 h (overnight) in dark.

2.5. Growth of gold nanoshells

An aliquot (e.g., 0.3 mL) of the gold-seeded silica nanoparticle solution prepared as described in Section 2.3 was injected into a vigorously stirred solution of gold salt (K-Gold solution; 24 mL). The thickness of the gold shell could be varied systematically by adjusting the amount of gold-seeded silica NP solution added. After stirring for 30 min, 40 μL of formaldehyde was injected slowly. Within 10 min, the solution changed from colorless to blue and then to dark red, which is characteristic of AuNS formation [5,11]. After 30 min, the nanoshells were centrifuged and then redispersed in HPLC grade water.

2.6. Surface functionalization of gold nanoshells

The aqueous AuNSs were mixed with 3-mercaptopropionic acid (MPA, 0.1 mol, 500:1 volume ratio of nanoshell solution:MPA) at room temperature to form a monolayer of MPA on the surface of the AuNSs. Excess MPA was then removed by two repetitive cycles of centrifugation (15 min, 1500 rpm) and redispersion of the nanoshells in deionized water. After removing the excess MPA, the MPA-functionalized AuNS solution was concentrated (×15) by centrifugation.

2.7. Preparation of PEI thin films containing gold nanoshells

A commercial solution of polyethyleneimine (PEI, 50 wt.% in H_2O) was diluted to 1 wt.% by adding deionized water. After cleaning by ultrasonication sequentially in soap, acetone, and water (10 min each), glass microscope slides were immersed in the 1 wt.% PEI solution for 1 h, and then washed with water and allowed to dry. The PEI films thus prepared were then immersed in the concentrated AuNS solution for several hours.

2.8. Characterization

The surface morphology of the AuNSs and overall uniformity of the composite films were examined by scanning electron microscopy (SEM). A JSM 6330F JEOL field emission scanning electron microscope was used at 15.0 kV. A variety of magnifications (×10,000–100,000) were employed to examine the product morphology. Extinction spectra were obtained using a Cary 50 Scan UV–vis spectrometer over the wavelength range of 300–1000 nm. Powder X-ray diffraction patterns

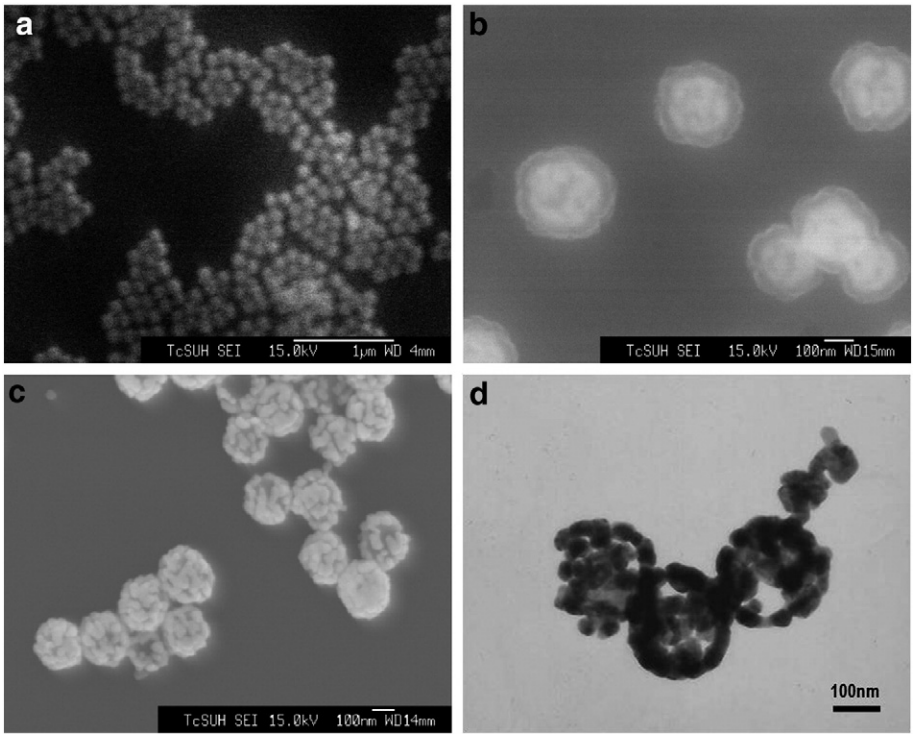

Fig. 1. SEM images of (a) silica particles and (b–c) gold nanoshells; (d) TEM image of gold nanoshells.

were obtained using a PANalytical X'Pert PRO diffractometer with Cu Kα radiation (λ = 1.54178 Å). The data were collected for 2θ ranging from 5–90° in 0.02° steps. X-ray photoelectron spectroscopy (XPS) analyses were carried out by using X-ray radiation from the aluminum K_α band. Spectra were recorded from 0 to 1100 eV and were internally calibrated by setting the $Au_{4f\ 7/2}$ binding energy to 84.0 eV.

3. Results and discussion

The purpose of this work was to develop a synthetic approach for fabricating AuNS thin films without particle aggregation or phase separation. The strategy for obtaining monolayer assembly of the AuNSs involves the attachment of a functionalized (charged) polymer on a flat substrate and the subsequent exposure of the AuNSs to an oppositely charged polyelectrolyte, facilitating the attachment via electrostatic forces.

Scheme 1 illustrates the process that we used to synthesize the AuNSs [11]. Silica (SiO_2) is a popular material used in shell/core particles because of its ease of synthesis, stability against coagulation, and versatility for functionalization [29,30]. This structural component is also chemically inert and optically transparent, and does not interfere with redox reactions at core surfaces. We prepared silica core particles via the hydrolysis and condensation of TEOS in the presence of ammonium hydroxide as a catalyst. We then functionalized the surface of the silica NPs by grafting with APTMS to give a terminal amine group on the surface. In a separate process, we prepared a colloidal gold solution via the reduction of hydrogen $HAuCl_4$ with THPC. The solution was then aged for several days in the refrigerator to allow the size of the nanoparticles to stabilize before being seeded onto the surface-functionalized silica core. The AuNP seeds produced by this method have consistently been observed to be ~2–3 nm in diameter [5,11]. The aged THPC-gold seeds were then deposited onto the silica particles by simple mixing. To grow the gold layer on the gold-seeded silica NPs, we prepared a solution containing a reducible gold salt (K-Gold). Gold shells were grown by adding the gold-seeded silica nanoparticles to the K-Gold solution. After stirring, AuNSs were produced having a diameter of ~200 nm.

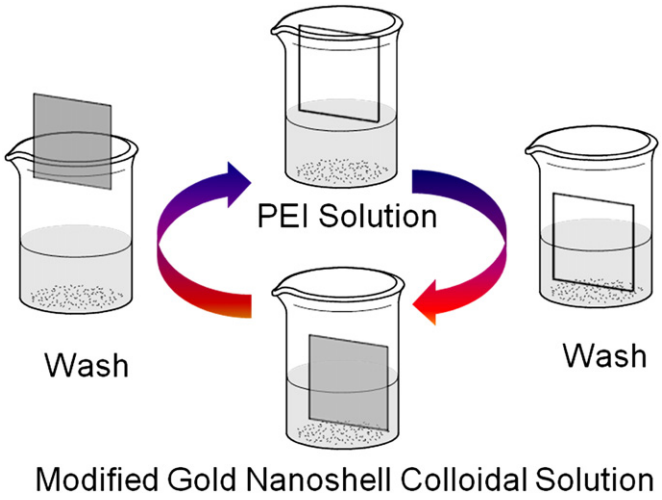

Scheme 2. Fabrication of nanoshell thin films by electrostatic layer-by-layer assembly.

The morphology of the silica particle cores and the AuNSs was investigated by SEM and transmission electron microscopy (TEM). The images in Fig. 1 show that the silica NPs are uniform in size (~150 nm). Similarly, the micrographs show that the nanoshells are spherical, but their surfaces are rough on the nanometer scale. Based on the SEM and TEM images, we can estimate the dimensions of these shell/core particles. Given that the silica core and AuNS diameters are ~150 nm and ~200 nm, respectively, we infer that the gold shells are ~25 nm thick. As a whole, the images in Fig. 1 provide direct evidence for the formation of AuNSs consisting of a silica core and a gold outer layer.

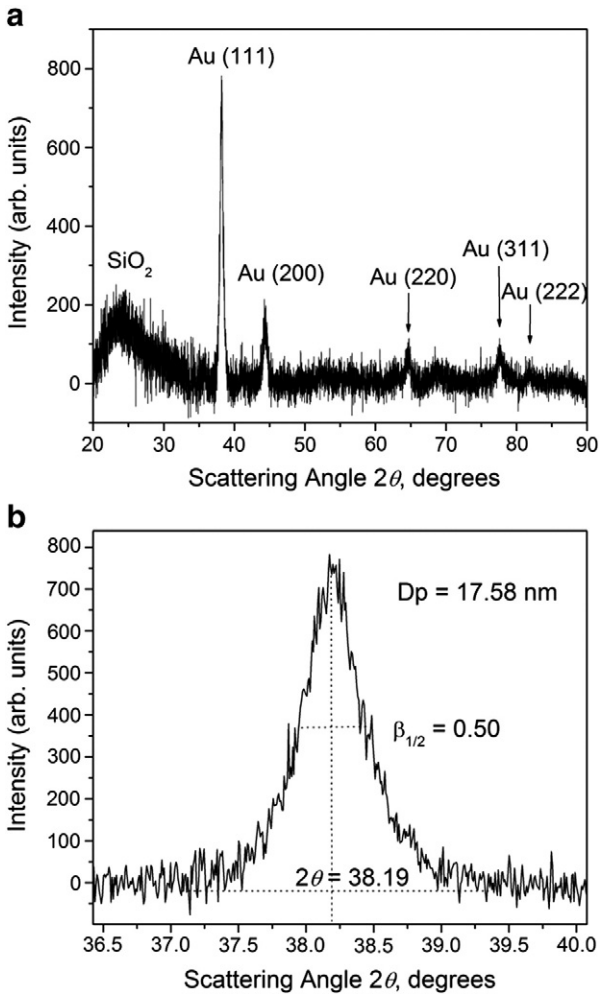

Fig. 2. X-ray diffraction pattern (a) of the gold nanoshells and (b) of a narrower range of angles at the (111) reflection peak for the crystallite size calculation using the Scherrer formula.

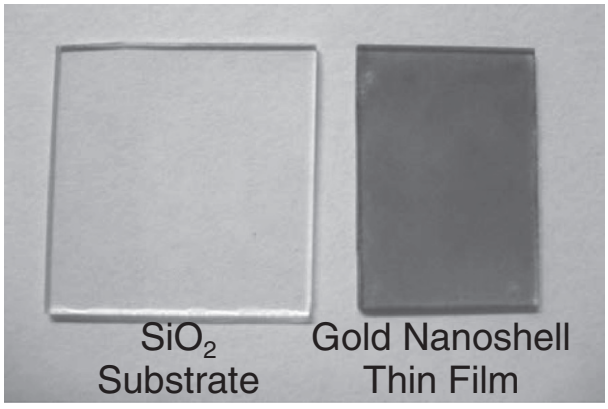

Fig. 3. This photo shows the bare SiO_2 substrate (left) and the AuNS/PEI film deposited on the SiO_2 substrate via the dip-coating process (right).

We used X-ray diffraction (XRD) to characterize further the AuNSs on the silica cores. The sharp peaks in Fig. 2a show that the outer layers are composed of crystalline gold, with $2\theta = 38.2°$, 44.3°, 64.7°, 77.6°, and 81.8°, corresponding to the (111), (200), (220), (311), and (222) lattice planes, respectively. The crystallite size of the gold shells was also determined from the (111) reflection in the XRD patterns using the Scherrer formula [31], as illustrated in Fig. 2b. The gold cluster size calculated using the Scherrer equation was ~17 nm, which is in reasonably good agreement with the shell thicknesses (~25 nm) determined from the SEM and TEM images in Fig. 1.

Scheme 2 shows the strategy we used to fabricate AuNS thin films via electrostatic layer-by-layer (LBL) assembly using simple dip-coating methods. To provide negatively charged particles, the nanoshells were functionalized by the addition of 3-mercaptopropionic

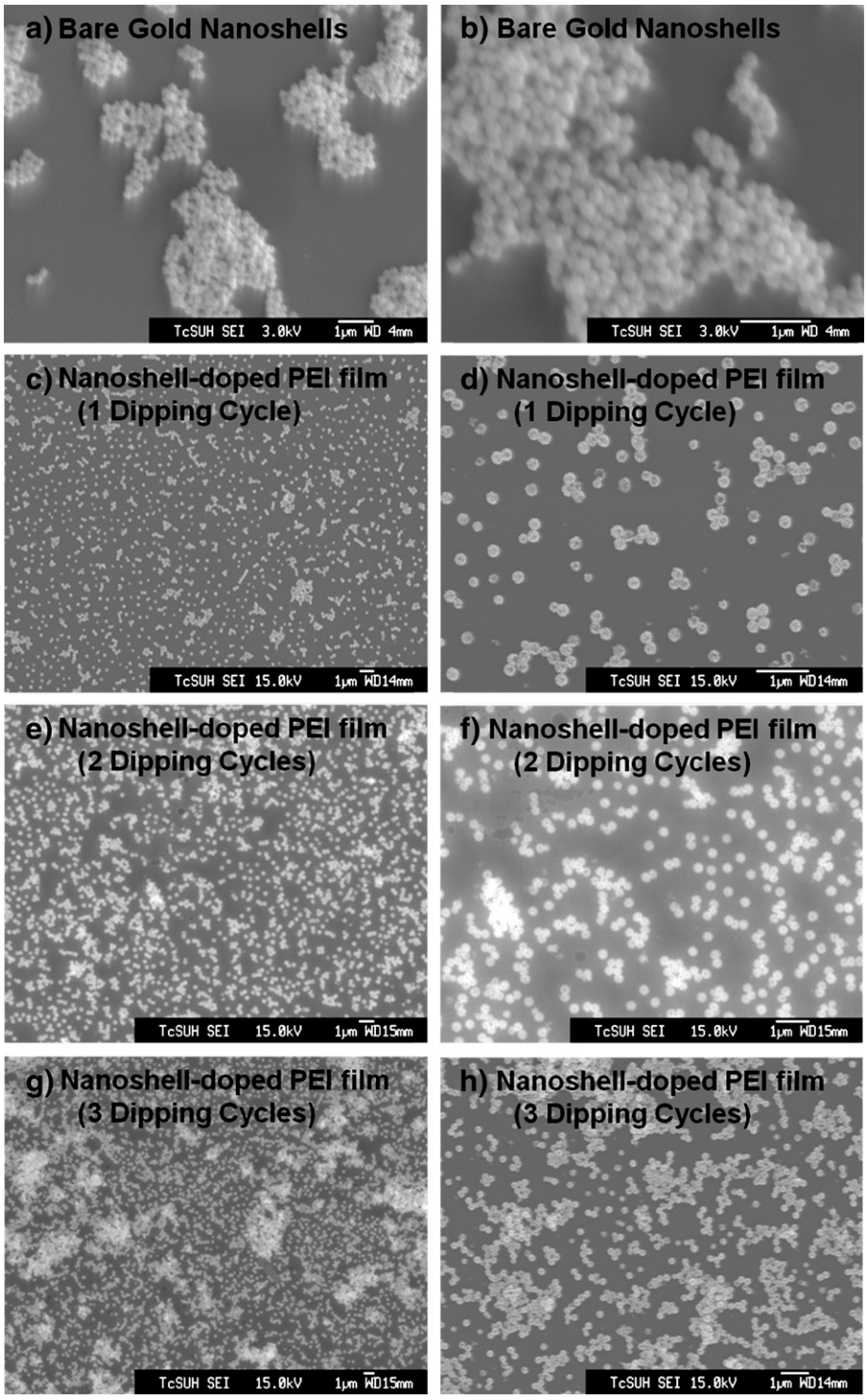

Fig. 4. SEM images of bare gold nanoshells (a–b) and nanoshells dispersed in PEI films after one dipping cycle(c–d), two dipping cycles (e–f), and three dipping cycles (g–h). Each set of images provides two different magnifications.

acid (MPA). The thiol (headgroup) covalently attached to the nanoshell surface through the strong sulfur and gold interaction [32]. Once the headgroups were bound to the gold, negatively charged carboxylate tailgroups formed upon exposure to the surrounding aqueous solution [33]. The introduction of MPA enhances the stability of the AuNSs through electrostatic repulsions [33], which enables the particles to be transferred from more highly concentrated nanoparticle solutions. After functionalization with MPA, no aggregation of the nanoshells was observed over several months. To give a positively charged surface [34], a thin film of PEI was adsorbed onto a glass substrate that had been thoroughly cleaned by ultrasonication. The cleaned substrate was immersed in 1 wt.% of PEI solution for 1 h, and then washed with water and dried under ambient conditions for several hours. The MPA-functionalized AuNSs were then adsorbed onto the PEI thin film. The negatively charged AuNSs readily adsorbed onto the positively charged PEI-coated surface by electrostatic attraction. The desired density of nanoshells on the surface was achieved by repeating the dipping process.

The image provided in Fig. 3 shows the resultant 2 cm × 3 cm AuNS/PEI thin film generated via the strategy shown in Scheme 2. The AuNS/PEI thin films are optically transparent, but exhibit a slightly gray color similar to tinted glass. Thus, efforts to increase the thickness of the AuNS/PEI film will be limited by the desired optical transparency of the resultant solar-to-thermal device. Future studies will seek to optimize solar collection and heat generation/transfer.

Fig. 4 shows representative SEM images of the AuNS-doped PEI films and the bare AuNSs deposited on a glass microscope slide. The images of the samples in Fig. 4a and b suggest that the nanoshells were significantly aggregated when the bare AuNSs were dropped onto the substrate. The nanoshells clustered together during the drying process, and as a consequence, some free space was produced on the surface. In contrast, by using the water-soluble polymer PEI, there was good particle dispersion, as confirmed by the separation between particles in Fig. 4c–h. The dipping process used to generate the MPA-functionalized AuNS-doped PEI films can be easily repeated, allowing the generation of thin films of nanoshells intercalated with PEI.

Scheme 3 illustrates the assembly process for generating the layer-by-layer assembled nanoshell films. The image of the samples generated after three dipping cycles of the AuNS/PEI thin films in Fig. 4 shows that the nanoshells appear to be more densely packed on the surface of the substrate, and when compared to the other images, the particles appear to agglomerate with an increasing number of dipping cycles. Given, however, that there is a PEI layer between each successive nanoshell layer as shown in Scheme 3, it seems likely that the SEM images simply show an increase in the total number of particles on the substrate, with the particles appearing to be near each other but separated vertically.

Fig. 5 shows the optical extinction spectra of the AuNSs in aqueous solution and the AuNS/PEI thin films in air. The SPR properties of AuNSs can be controlled by varying the core size and shell thickness [32]. The SPR peak of the aqueous AuNSs prepared by the procedure described above was 720 nm (Fig. 5a). The extinction maximum for the AuNS/PEI thin films was broadened and shifted to longer wavelength (800 nm) (Fig. 5b). The position of the surface plasmon resonance is sensitive to the dielectric environment, and as the refraction index increases, the peak red-shifts and broadens [35]. Therefore, the observed red shift in Fig. 5 is consistent with coating the nanoparticles with a high refractive index material such as PEI (1.529) [36], which is higher than that of water (1.333) [35]. Additionally, the SPR band of the nanoshells embedded in the PEI film after 3 dipping cycles red-shifts further to 875 nm due to the increased number of AuNSs. More

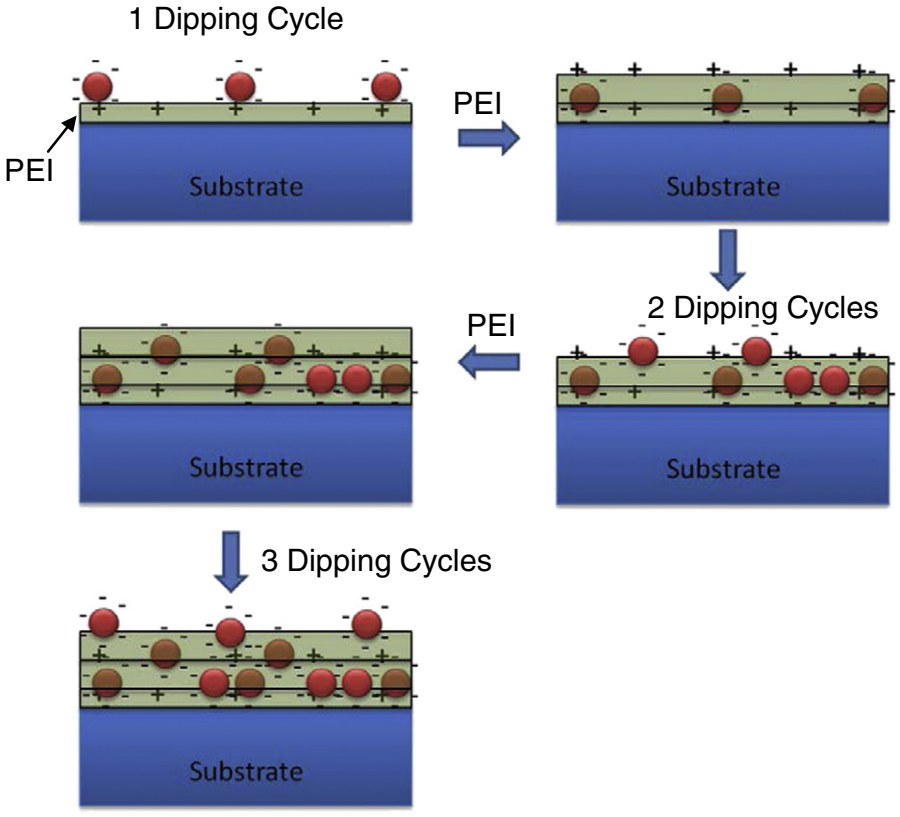

Scheme 3. Illustration of the layer-by-layer assembly process.

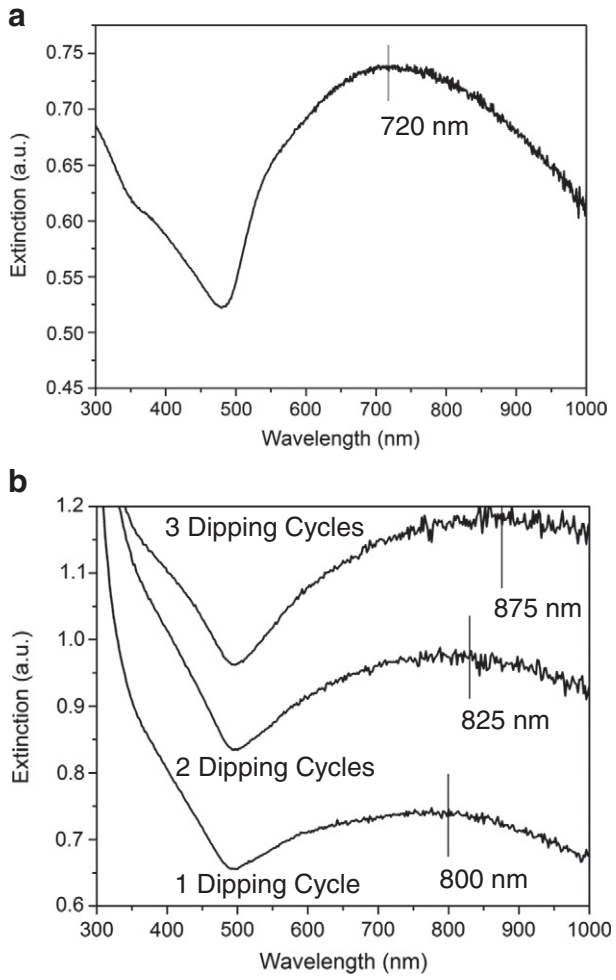

Fig. 5. UV–vis spectra of gold nanoshells (a) in aqueous solution and (b) incorporated in AuNS/PEI films as a function of the number of dipping cycles.

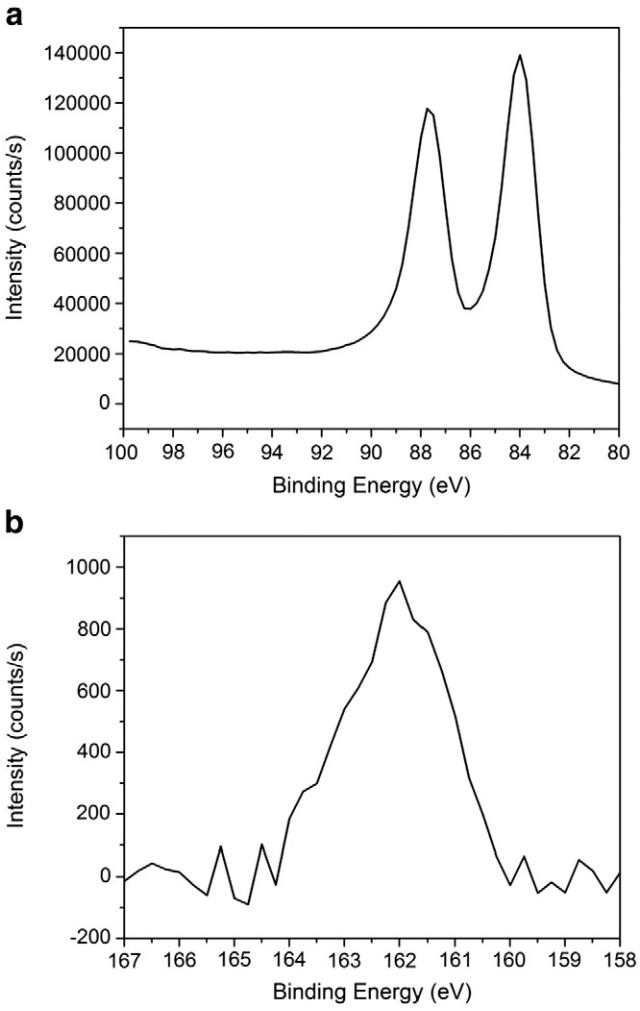

Fig. 6. High-resolution XPS spectra of an AuNS-PEI film for (a) the Au_{4f} and (b) the S_{2p} regions.

precisely, when compared to dispersions in solution, a localized increase in the particle density in the film can plausibly give rise to a broadening and red-shifting of the surface plasmon band [37]. With a reduction in distance between AuNSs, the dipolar surface plasmons of the individual nanoshells can strongly intermix to form a hybridized plasmon band, which disperses strongly to lower energies corresponding to higher wavelengths [37]. Therefore, for our samples, the SPR peak position slightly red-shifted with an increase in the number of the dipping cycles, as shown in Fig. 5b, which is consistent with an increase in the number of particles in close proximity to each other within the film. The intensity of the band also increased with an increase in the number of dipping cycles, which is likely owing to the corresponding increase in the number of nanoshell particles in the films.

Fig. 6 shows the XPS spectra of the AuNS film corresponding to the high-resolution core level data for Au_{4f} and S_{2p}, with the $Au_{4f\ 7/2}$ peak referenced to 84.0 eV. After the introduction of MPA onto the surface of the nanoshells, the newly formed Au-S covalent bond was verified by analysis of the atomic binding energy for the S_{2p} electrons for sulfur. In particular, the S_{2p} region of the XPS spectra can be used to evaluate Au–S bond formation because of differences between the bound sulfur atom as compared to the unbound sulfur atom: the binding energy of the $S_{2p\ 3/2}$ peak appears at ~162.1 eV and ~163.6 eV for S bound to Au surfaces and unbound thiols, respectively [38]. As shown in Fig. 6b, the strong intensity of the $S_{2p\ 3/2}$ peak at ~162 eV for the bound thiolate sulfur suggests covalent bonding between the thiol and gold [38]. Based on these data, XPS confirms the introduction of MPA groups on the surface of the AuNSs and that the chemically bound surfactant remains an integral component in the final thin film assembly.

4. Conclusions

We have demonstrated the synthesis of gold nanoshells via the "seeded growth" method and the fabrication of polymer-dispersed AuNS thin films via electrostatic layer-by-layer assembly by way of simple dip-coating techniques. Negatively charged MPA-coated AuNSs were adsorbed electrostatically onto positively charged PEI-coated glass substrates. Thin films were formed by alternately dipping the glass slides in PEI solution and in a solution containing the modified AuNSs. This method produced AuNS/PEI films that exhibited limited aggregation and proved to have a good distribution of particles, as determined by SEM. The peak position of the SPR band for each film was affected by the number of layers of deposited AuNSs. An increase in localized particle density due to the increase in the number of dipping cycles can plausibly give rise to the observed shift. The resulting decrease in distance between AuNSs produced a red-shift for the surface plasmon band because the dipolar plasmons of the nanoshells could then strongly intermix to form hybridized plasmon bands, which disperse strongly to lower energies (longer wavelengths). The intensities of the extinction bands of the films were also directly proportional to the number of dipping cycles because of the increase in the number of particles deposited

on the surface. XPS analysis of the final thin film indicates that the surfactants on the AuNSs are chemically bound to the gold and that these bonds remain intact after completion of the thin film assembly process. Overall, water-soluble PEI polymer proved to be an effective medium for AuNS dispersion within films produced by layer-by-layer deposition processes because it was readily adsorbed on the glass substrate and produced assemblies having well distributed AuNSs.

Acknowledgment

The Robert A. Welch Foundation (Grants E-1206, E-0024, and E-1320) and the Texas Center for Superconductivity at the University of Houston provided generous support for this research.

References

[1] P.C. Chen, S.C. Mwakwari, A.K. Oyelere, Gold nanoparticles: From nanomedicine to nanosensing, Nanotechnol. Sci. Appl. 1 (2008) 45.
[2] P.N. Prasad, Nanophotonics, Wiley-Interscience, New York, 2004.
[3] M.R. Jones, K.D. Osberg, R.J. Macfarlane, M.R. Langille, C.A. Mirkin, Templated techniques for the synthesis and assembly of plasmonic nanostructures, Chem. Rev. 111 (2011) 3736.
[4] S. Link, Z.L. Wang, M.A. El-Sayed, Alloy formation of gold-silver nanoparticles and the dependence of the plasmon absorption on their composition, J. Phys. Chem. B 103 (18) (1999) 3529.
[5] J.-H. Kim, W.W. Bryan, T.R. Lee, Preparation, characterization, and optical properties of gold, silver, and gold-silver alloy nanoshells having silica cores, Langmuir 24 (19) (2008) 11147.
[6] K.-T. Yong, Y. Sahoo, M.T. Swihart, P.N. Prasad, Synthesis and plasmonic properties of silver and gold nanoshells on polystyrene cores of different size and of gold-silver core-shell nanostructures, Colloids Surf. A Physicochem. Eng. Asp. 290 (1–3) (2006) 89.
[7] S.J. Oldenburg, R.D. Averitt, S.L. Westcott, N.J. Halas, Nanoengineering of optical resonances, Chem. Phys. Lett. 288 (2,3,4) (1998) 243.
[8] K.L. Kelly, E. Coronado, L.L. Zhao, G.C. Schatz, The optical properties of metal nanoparticles: The influence of size, shape, and dielectric environment, J. Phys. Chem. B 107 (2003) 668.
[9] H.H. Richardson, M.T. Carlson, P.J. Tandler, P. Hernandez, A.O. Govorov, Experimental and theoretical studies of light-to-heat conversion and collective heating effects in metal nanoparticle solutions, Nano Lett. 9 (3) (2009) 1139.
[10] H.H. Richardson, Z.N. Hickman, A.O. Govorov, A.C. Thomas, W. Zhang, M.E. Kordesch, Thermooptical properties of gold nanoparticles embedded in ice: Characterization of heat generation and melting, Nano Lett. 6 (4) (2006) 783.
[11] T. Pham, J.B. Jackson, N.J. Halas, T.R. Lee, Preparation and characterization of gold nanoshells coated with self-assembled monolayers, Langmuir 18 (12) (2002) 4915.
[12] R.D. Averitt, D. Sarkar, N.J. Halas, Plasmon resonance shifts of Au-coated Au_2S nanoshells: Insight into multicomponent nanoparticle growth, Phys. Rev. Lett. 78 (22) (1997) 4217.
[13] H. Liu, T. Liu, X. Wu, L. Li, L. Tan, D. Chen, F. Tang, Targeting gold nanoshells on silica nanorattles: A drug cocktail to fight breast tumors via a single irradiation with near-infrared laser light, Adv. Mater. 24 (6) (2012) 755.
[14] B. Kuestner, M. Gellner, M. Schutz, F. Schoppler, A. Marx, P. Strobel, P. Adam, C. Schmuck, S. Schlucker, SERS labels for red laser excitation: Silica-encapsulated SAMs on tunable gold/silver nanoshells, Angew. Chem. Int. Ed. 48 (11) (2009) 1950.
[15] C. Loo, A. Lowery, N. Halas, J. West, R. Drezek, Immunotargeted nanoshells for integrated cancer imaging and therapy, Nano Lett. 5 (4) (2005) 709.
[16] A.M. Gobin, M.H. Lee, N.J. Halas, W.D. James, R.A. Drezek, J.L. West, Near-infrared resonant nanoshells for combined optical imaging and photothermal cancer therapy, Nano Lett. 7 (7) (2007) 1929.
[17] S.-Y. Liu, Z.-S. Liang, F. Gao, S.-F. Luo, G.-Q. Lu, *In vitro* photothermal study of gold nanoshells functionalized with small targeting peptides to liver cancer cells, J. Mater. Sci. Mater. Med. 21 (2) (2010) 665.
[18] P.K. Jain, X. Huang, I.H. El-Sayed, M.A. El-Sayed, Noble metals on the nanoscale: Optical and photothermal properties and some applications in imaging, sensing, biology, and medicine, Acc. Chem. Res. 41 (12) (2008) 1578.
[19] Y. Rao, Q. Chen, J. Dong, W. Qian, Growth-sensitive 3D ordered gold nanoshells precursor composite arrays as SERS nanoprobes for assessing hydrogen peroxide scavenging activity, Analyst 136 (2011) 769.
[20] R.G. Chaudhuri, S. Paria, Core/shell nanoparticles: Classes, properties, synthesis mechanisms, characterization, and applications, Chem. Rev. 112 (2012) 2373.
[21] J. Schmitt, G. Decher, W.J. Dressick, S.L. Brandow, R.E. Geer, R. Shashidhar, J.M. Calvert, Metal nanoparticle/polymer superlattice films. Fabrication and control of layer structure, Adv. Mater. 9 (1997) 61.
[22] J. Kim, S.W. Lee, P.T. Hammond, Y. Shao-Horn, Electrostatic layer-by-layer assembled Au nanoparticle/MWNT thin films: Microstructure, optical property, and electrocatalytic activity for methanol oxidation, Chem. Mater. 21 (13) (2009) 2993.
[23] F.N. Crespilho, V. Zucolotto, C.M.A. Brett, O.N. Oliveira Jr., F.C. Nart, Enhanced charge transport and incorporation of redox mediators in layer-by-layer films containing PAMAMencapsulated gold nanoparticles, J. Phys. Chem. B 110 (35) (2006) 17478.
[24] Y. Huang, Y. Yang, Z. Chen, X. Li, M. Nogami, Fabricating Au-Ag core-shell composite films for surface-enhanced raman scattering, J. Mater. Sci. 43 (15) (2008) 5390.
[25] F. Zhang, M.P. Srinivasan, Layer-by-layer assembled gold nanoparticle films on amineterminated substrates, J. Colloid Interface Sci. 319 (2) (2008) 450.
[26] I.U. Vakarelski, R. Maenosono, J.W. Kwek, K. Higashitani, Thermal modification of layer-by- layer assembled gold nanoparticle films, Colloids Surf. A Physicochem. Eng. Asp. 340 (2009) 193.
[27] B.J. Lee, K. Park, T. Walsh, L. Xu, Radiative heat transfer analysis in plasmonic nanofluids for direct solar thermal absorption, J. Sol. Energy Eng. 134 (2) (2012) (021009/1-6).
[28] M.D. Brown, T. Suteewong, R.S.S. Kumar, V. D'Innocenzo, A. Petrozza, M. Lee, U. Wiesner, H.J. Snaith, Plasmonic dye-sensitized solar cells using core-shell metal-insulator nanoparticles, Nano Lett. 11 (2) (2011) 438.
[29] S. Kalele, S.W. Gosavi, J. Urban, S.K. Kulkarni, Nanoshell particles: Synthesis, properties and applications, Curr. Sci. 91 (8) (2006) 1038.
[30] T. Ung, L.M. Liz-Marzan, P. Mulvaney, Controlled method for silica coating of silver colloids. Influence of coating on the rate of chemical reactions, Langmuir 14 (14) (1998) 3740.
[31] B.D. Cullity, Elements of X-Ray Diffraction, Addison-Wesley, MA, USA, 1977.
[32] R.G. Nuzzo, F.A. Fusco, D.L. Allara, Spontaneously organized molecular assemblies. 3. Preparation and properties of solution adsorbed monolayers of organic disulfides on gold surfaces, J. Am. Chem. Soc. 109 (8) (1987) 2358.
[33] J. Gao, X. Huang, H. Liu, F. Zan, J. Ren, Colloidal stability of gold nanoparticles modified with thiol compounds: Bioconjugation and application in cancer cell imaging, Langmuir 28 (9) (2009) 4464.
[34] A. Carrillo, J.A. Swartz, J.M. Gamba, R.S. Kane, N. Chakrapani, B. Wei, P.M. Ajayan, Noncovalent functionalization of graphite and carbon nanotubes with polymer multilayers and gold nanoparticles, Nano Lett. 3 (10) (2003) 1437.
[35] C. Noguez, Surface plasmons on metal nanoparticles: The influence of shape and physical environment, J. Phys. Chem. C 111 (10) (2007) 3806.
[36] R. Teixeira, P.M.R. Paulo, A.S. Viana, S.M.B. Costa, Plasmon-enhanced emission of a phthalocyanine in polyelectrolyte films induced by gold nanoparticles, J. Phys. Chem. C 115 (50) (2011) 24674.
[37] H. Wang, J. Kundu, N.J. Halas, Plasmonic nanoshell arrays combine surface-enhanced vibrational spectroscopies on a single substrate, Angew. Chem. Int. Ed. 46 (47) (2007) 9040.
[38] D.G. Castner, K. Hinds, D.W. Grainger, X-ray photoelectron spectroscopy sulfur 2p study of organic thiol and disulfide binding interactions with gold surfaces, Langmuir 12 (21) (1996) 5083.